Numerical Simulation of Three-phase Flow in Heterogeneous Porous Media

Eduardo Abreu[1]**, Frederico Furtado[2], and Felipe Pereira[1]

[1] Universidade do Estado do Rio de Janeiro,
Nova Friburgo, RJ 25630-050, Brazil,
eabreu@iprj.uerj.br, pereira@iprj.uerj.br
WWW home page: http://www.labtran.iprj.uerj.br
[2] University of Wyoming, Laramie 82071-3036, USA,
furtado@uwyo.edu
WWW home page: http://www.uwyo.edu/furtado/

Abstract. We describe an efficient numerical simulator, based on an operator splitting technique, for three-phase flow in heterogeneous porous media that takes into account capillary forces, general relations for the relative permeability functions and variable porosity and permeability fields. Our numerical procedure combines a non-oscillatory, second order, conservative central difference scheme for the system of hyperbolic conservation laws modeling the convective transport of the fluid phases with locally conservative mixed finite elements for the approximation of the parabolic and elliptic problems associated with the diffusive transport of fluid phases and the pressure-velocity calculation. This numerical procedure has been used to investigate the existence and stability of non-classical waves (also called transitional or undercompressive waves) in heterogeneous two-dimensional flows, thereby extending previous results for one-dimensional problems.

1 Introduction

Three-phase flow in porous media is important in a number of scientific and technological contexts. Examples include gas injection and thermal flooding in oil reservoirs, flow of non-aqueous phase liquids in the vadose zone, and radio-nuclide migration from repositories of nuclear waste. In this paper we are concerned with the accurate numerical simulation of three-phase flow in heterogeneous porous media.

Three-phase flow in a porous medium can be modeled, using Darcy's law, in terms of the relative permeability functions of the three fluid phases (say, oil, gas, and water). Distinct empirical models have been proposed for the relative permeability functions [10, 13, 26, 17]. It is well known that for some of these models [10, 26], which have been used extensively in petroleum engineering, the 2×2 system of conservation laws (the saturation equations) that arises

** Candidate to the Best Student Paper Award

when capillarity (diffusive) effects are neglected fails to be strictly hyperbolic somewhere in the interior of the saturation triangle (the phase space). This loss of strict hyperbolicity leads to the frequent occurrence of non-classical waves (also called transitional or undercompressive shock waves) in the solutions of the three-phase flow model. Crucial to calculating transitional shock waves is the correct modeling of capillarity effects [15].

We describe a numerical procedure, based on a two-level operator splitting technique, for three-phase flow that takes into account capillary pressure differences. This procedure combines a non-oscillatory, second order, conservative central difference scheme, introduced by Nessyahu-Tadmor (NT) [24], for the numerical approximation of the system of conservation laws describing the convective transport of the fluid phases with locally conservative mixed finite elements for the approximation of the parabolic and elliptic problems associated with the diffusive transport of fluid phases and the pressure-velocity calculation [23] (see also [2–4]).

This numerical procedure has been used to indicate the existence of non-classical transitional waves in multidimensional heterogeneous flows (see [3, 4] for preliminary computational results), thereby extending previous results for one-dimensional problems [22, 2]. The authors are currently investigating, with the numerical procedure developed, the existence and stability (with respect to viscous fingering) of transitional waves in heterogeneous formations as a first step in the analysis of the scale-up problem for three-phase flow.

We list four distinctive aspects of our numerical scheme:

- Dimensional splitting is unnecessary. Recently, a "corrected" time-splitting method for one-dimensional nonlinear convection-diffusion problems was introduced in [18, 19] to better account for the delicate balance between the focusing effects of nonlinear convection, which lead to the formation of shocks, and the smoothing effects of diffusion. As a consequence, this new method reduces considerably the error associated with viscous splitting, allowing accurate large time-steps to be taken in the computation. However, the extension of this method to multidimensional problems requires the use of dimensional splitting. It is known that in the presence of strong multidimensional effects the errors of dimensional splitting might be large (see [9]).
- Riemann solvers or approximate Riemann solvers are unnecessary.
- A CFL time-step restriction applies only to the hyperbolic part of the calculation. The parabolic part of the calculation is performed implicitly, and does not restrict the size of the time-steps for stability.
- We compute accurate velocity fields in the presence of highly variable permeability fields by discretizing the elliptic equation with mixed finite elements.

Different approaches for solving numerically the three-phase flow equations are discussed in [5, 7, 21].

The rest of this paper is organized as follows. In Section 2 we introduce the model for three-phase flow in heterogeneous porous media that we consider. In Section 3 we discuss strategies for solving the hyperbolic and diffusive problems

taking into account variable porosity fields. In Section 4 we present computational solutions for the model problem considered here. Conclusions appear in section 5.

2 Governing equations for Three-Phase Flows

We consider two-dimensional, horizontal flow of three immiscible fluid phases in a porous medium. The phases will be refereed to as water, gas, and oil and indicated by the subscripts w, g, and o, respectively. We assume that there are no internal sources or sinks. Compressibility, mass transfer between phases, and thermal effects are neglected.

We assume that the three fluid phases saturate the pores; thus, with S_i denoting the saturation (local volume fraction) of phase i, $\sum_i S_i = 1$, $i = g, o, w$. Consequently, any pair of saturations inside the triangle of saturations $\triangle := \{ (S_i, S_j) : S_i, S_j \geq 0, S_i + S_j \leq 1, i \neq j\}$ can be chosen to describe the state of the fluid.

We refer the reader to [25, 3] for a detailed description of the derivation of the phase formulation of the governing equations of three-phase flow. In our model we shall work with the saturations S_w and S_g of water and gas, respectively. Then, the equations governing the three-phase flow are as follows:

Saturation equations:

$$\frac{\partial}{\partial t}(\phi(\mathbf{x})S_w) + \nabla \cdot (\mathbf{v} f_w(S_w, S_g)) = \nabla \cdot \mathbf{w}_w \tag{1}$$

$$\frac{\partial}{\partial t}(\phi(\mathbf{x})S_g) + \nabla \cdot (\mathbf{v} f_g(S_w, S_g)) = \nabla \cdot \mathbf{w}_g. \tag{2}$$

The diffusion terms $\mathbf{w}_w$ and $\mathbf{w}_g$ that arise because of capillary pressure differences are given by

$$[\mathbf{w}_w, \mathbf{w}_g]^T = K(\mathbf{x})\, B(S_w, S_g)\, [\nabla S_w, \nabla S_g]^T . \tag{3}$$

Here, $[\mathbf{a}, \mathbf{b}]$ denotes the 2-by-2 matrix with column vectors $\mathbf{a}$ and $\mathbf{b}$, and $B(S_w, S_g) = QP'$, where

$$Q(S_w, S_g) = \begin{bmatrix} \lambda_w(1 - f_w) & -\lambda_w f_g \\ -\lambda_g f_w & \lambda_g(1 - f_g) \end{bmatrix}, \quad P'(S_w, S_g) = \begin{bmatrix} \dfrac{\partial p_{wo}}{\partial S_w} & \dfrac{\partial p_{wo}}{\partial S_g} \\ \dfrac{\partial p_{go}}{\partial S_w} & \dfrac{\partial p_{go}}{\partial S_g} \end{bmatrix}. \tag{4}$$

In the above, $K(\mathbf{x})$ and $\phi(\mathbf{x})$ are the absolute permeability and the rock porosity of the porous medium, respectively. $\lambda_i(S_w, S_g) = k_i/\mu_i$, $i = w, g$, denote the phase mobilities, given in terms of the phase relative permeabilities k_i and phase viscosities μ_i. The fractional flow function of phase i is given by $f_i(S_w, S_g) = \lambda_i/\lambda$. The capillary pressures $p_{ij} = p_i - p_j$, $i \neq j$, where p_i is the pressure in phase i, are assumed to depend solely on the saturations.

Pressure-Velocity equations:

$$\nabla \cdot \mathbf{v} = 0, \tag{5}$$

$$\mathbf{v} = -K(\mathbf{x})\lambda(S_w, S_g)\nabla p_o + \mathbf{v}_{wo} + \mathbf{v}_{go}, \tag{6}$$

where $\mathbf{v}_{wo}$ and $\mathbf{v}_{go}$ are "correction velocities" defined by

$$\mathbf{v}_{ij} = -K(\mathbf{x})\lambda_i(S_w, S_g)\nabla p_{ij}. \tag{7}$$

Boundary and initial conditions for the system of equations (1)-(7) must be imposed to complete the definition of the mathematical model. In particular, S_w and S_g must be specified at the initial time $t = 0$.

3 The Numerical Simulator

We employ a two-level operator-splitting procedure for the numerical solution of the three-phase flow system (1)-(7). Operator splitting techniques constitute one of the several bridges between numerical and functional analysis. In numerical analysis, they represent algorithms intended to approximate evolution equations accurately in a computationally efficient fashion. In functional analysis, they are used to prove estimates, existence and representation theorems. The survey article [8] discusses both uses and point to a large bibliography.

The splitting technique discussed here allows for time steps for the pressure-velocity calculation that are longer than those for the diffusive calculation, which, in turn, can be longer than those for advection. Thus, we introduce three time steps: Δt_c for the solution of the hyperbolic problem for the advection, Δt_d for the solution of the parabolic problem for the diffusive calculation and Δt_p for the elliptic problem for the pressure-velocity calculation, so that $\Delta t_p \geq \Delta t_d \geq \Delta t_c$. We remark that in practice variable time steps are always useful, especially for the advection micro-steps subject dynamically to a CFL condition.

The oil pressure and the Darcy velocity, Eqs. (5)-(7), are approximated at times $t^m = m\Delta t_p$, $m = 0, 1, 2, \ldots$ using locally conservative mixed finite elements (see [3]). The linear system of algebraic equations that arises from the discretization can be solved by a preconditioned conjugate gradient procedure (PCG) or by a domain decomposition procedure [11, 4, 3].

The saturations S_w and S_g are approximated at times $t_n = n\Delta t_d$, $n = 1, 2, \ldots$ in the diffusive calculation; recall that they are specified at $t = 0$. For $t > 0$ these values are obtained from last solution of the hyperbolic subsystem of conservation laws modeling the convective transport of the fluid phases. In this stage the parabolic subsystem associated to the system (1)-(4) is solved. Locally conservative mixed finite elements are used to discretize the spatial operators in the diffusion system. The time discretization of the latter is performed by means of the implicit backward Euler method (see [3]).

In addition, there are values for the saturations computed at intermediate times $t_{n,\kappa} = t_n + k\Delta t_c$ for $t_n < t_{n,\kappa} \leq t_{n+1}$ that take into account the convective transport of water and gas but ignore the diffusive effects. In these intermediate

times the subsystem of nonlinear conservation laws is approximated by a non-oscillatory, second order, conservative central difference scheme (see [24, 3]).

We refer to [3, 2] for a detailed description of the fractional-step procedure.

3.1 The NT central scheme for variable porosity fields

In this section we discuss a possible implementation of the NT central differencing scheme for variable porosity fields (see [24] for the original scheme) and its application to the solution of the hyperbolic subsystem associated with system (1)-(4). For brevity, we only discuss the ideas for a scalar conservation law and in one space dimension. The simplicity of the extension of the ideas to systems of equations, by a component-wise application of the scalar scheme, and to multi-dimensions is one of the hallmarks of the NT scheme.

The key features of the NT scheme are: a non-oscillatory, piecewise linear (bilinear in two-space dimension) reconstruction of the solution point-values from their given cell averages and central differencing based on the *staggered* evolution of the reconstructed averages.

Consider the following scalar conservation law,

$$\frac{\partial}{\partial t}(\phi\, s) + \frac{\partial}{\partial x} f(s) = 0, \tag{8}$$

where $\phi = \phi(x)$ is the porosity and $s = s(x,t)$ is the saturation (the volume fraction of one of the fluid phases). At each time level, a piecewise constant approximate solution over cells of width $\Delta x = x_{j+\frac{1}{2}} - x_{j-\frac{1}{2}}$ (see Figure 1),

$$\overline{s}(x,t) = s_j(t), \qquad x_{j-\frac{1}{2}} \le x \le x_{j+\frac{1}{2}}, \tag{9}$$

is first reconstructed by a piecewise linear approximation of the form

$$L_j(x,t) = s_j(t) + (x - x_j)\frac{1}{\Delta x} s'_j(t), \quad x_{j-\frac{1}{2}} \le x \le x_{j+\frac{1}{2}}, \tag{10}$$

using nonlinear MUSCL-type slope limiters (see [24] and references therein) to prevent oscillations. This reconstruction compensates the excessive numerical diffusion of central differencing. We observe that (9) and (10) can be interpreted as grid projections of solutions of successive noninteracting Riemann problems which are integrated over a staggered grid ($x_j \le x \le x_{j+1}$; see Figure 1). The form (10) retains conservation, i.e., (here the over-bar denotes the $[x_{j-\frac{1}{2}}, x_{j+\frac{1}{2}}]$-cell average),

$$\bar{L}_j(x,t) = \bar{s}(x,t) = s_j(t). \tag{11}$$

Second-order accuracy is guaranteed if the numerical derivatives, defined as $\frac{1}{\Delta x} s'_j$, satisfy (see [24]):

$$\frac{1}{\Delta x} s'_j(t) = \frac{\partial}{\partial x} s(x = x_j, t) + O(\Delta x). \tag{12}$$

In the second stage, the piecewise linear interpolant (10) is evolved in time through the solution of successive noninteracting Generalized Riemann (GR) problems (see Figure 1),

$$s(x, t + \Delta t_c) = GR(x, t + \Delta t_c; L_j(x,t), L_{j+1}(x,t)), \;\; x_j < x < x_{j+1}. \tag{13}$$

The resulting solution (13) is then projected back into the space of staggered piecewise constant grid-functions to yield

$$s_{j+\frac{1}{2}}(t + \Delta t_c)\phi_{j+\frac{1}{2}} \;\equiv\; \frac{1}{\Delta x}\int_{x_j}^{x_{j+1}} \phi(x) s(x, t + \Delta t_c)\, dx, \tag{14}$$

where $\phi_{j+\frac{1}{2}}$ is the average value of $\phi(x)$ on the cell $[x_j, x_{j+1}]$. In view of the conservation law (8),

$$\begin{aligned} s_{j+\frac{1}{2}}(t + \Delta t_c)\phi_{j+\frac{1}{2}} = \frac{1}{\Delta x}\Big[\int_{x_j}^{x_{j+\frac{1}{2}}} \phi(x) L_j(x,t)\, dx + \int_{x_{j+\frac{1}{2}}}^{x_{j+1}} \phi(x) L_{j+1}(x,t)\, dx\Big] \\ -\frac{1}{\Delta x}\Big[\int_t^{t+\Delta t_c} f(s(x_{j+1},\tau))\, d\tau - \int_t^{t+\Delta t_c} f(s(x_j,\tau))\, d\tau\Big]. \end{aligned} \tag{15}$$

The first two integrands on the right of (15), $L_j(x,t)$ and $L_{j+1}(x,t)$, can be integrated exactly. We remark that the porosity is assumed to be constant on cells, $\phi(x) = \phi_j$ for $x_j \le x \le x_{j+1}$. Moreover, if the CFL condition

$$\frac{\Delta t_c}{\Delta x} \max_{x_j \le x \le x_{j+1}} \left\{ \frac{f'(s(x,t))}{\phi(x)} \right\} < \frac{1}{2}, \tag{16}$$

holds, then the last two integrands on the right of (15) are smooth functions of τ. Hence, they can be integrated approximately by the midpoint rule, at the expense of an $O(\Delta t^3)$ local truncation error, to yield the following corrector step,

$$\begin{aligned} & s_{j+\frac{1}{2}}(t + \Delta t_c)\phi_{j+\frac{1}{2}} = \frac{1}{2}[\phi_j s_j(t) + \phi_{j+1} s_{j+1}(t)] + \frac{1}{8}[\phi_j s'_j(t) - \phi_{j+1} s'_{j+1}(t)] \\ & -\alpha_x \left[f\left(s\left(x_{j+1}, t + \tfrac{\Delta t_c}{2}\right)\right) - f\left(s\left(x_j, t + \tfrac{\Delta t_c}{2}\right)\right)\right], \end{aligned} \tag{17}$$

where $\alpha_x = \Delta t_c / \Delta x$.

We observe that the spatial integration in (15) is performed over the entire Riemann fan, which consists of both left- and right-going waves. This is the distinctive feature of the NT scheme. On the one hand, this integration eliminates the need of any detailed knowledge about the exact (or approximate) generalized Riemann solver $GR(\cdot;\cdot,\cdot)$; on the other hand, it facilitates accurate computation of the numerical flux, $\int_t^{t+\Delta t_c} f(s(x_j,\tau))d\tau$, whose values are extracted from the smooth interface of two noninteracting generalized Riemann problems (see Figure 1).

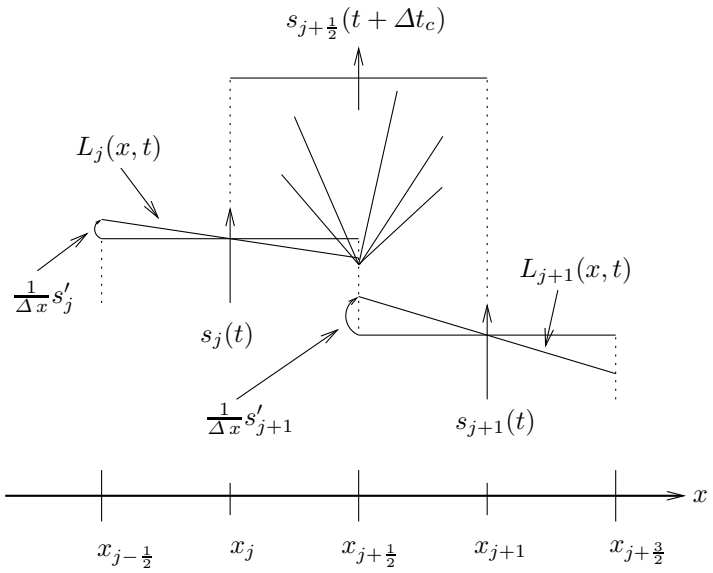

Fig. 1. Evolution from the time level t to the time level $t + \Delta t_c$. The porosity is assumed to be piecewise constant, with constant values on the cells of the original grid: $\phi(x) = \phi_j$, $x_{i-1/2} \le x \le x_{i+1/2}$.

By Taylor expansion and the conservation law (8),

$$s(x_j, t + \Delta t_c/2) = s_j(t) - \frac{1}{2\phi_j}\alpha_x f'_j(t), \tag{18}$$

may serve (as predictor step) for the approximation of the saturation mid-values of the numerical fluxes that appears in (17) within the permissible second-order accuracy requirement. Here, $\frac{1}{\Delta x}f'_j$ stands for an approximate numerical derivative of the numerical flux $f(s(x = x_j, t))$,

$$\frac{1}{\Delta x}f'_j(t) = \frac{\partial}{\partial x}(f(s(x = x_j, t))) + O(\Delta x). \tag{19}$$

Next, a piecewise linear interpolant is reconstructed

$$L_{j+\frac{1}{2}}(x, t+\Delta t_c) = s_{j+\frac{1}{2}}(t+\Delta t_c) + (x - x_{j+\frac{1}{2}})\frac{1}{\Delta x}s'_{j+\frac{1}{2}}(t + \Delta t_c),\ x_j \le x \le x_{j+1}, \tag{20}$$

again using nonlinear slope limiters, and then averaged over the original grid to yield the non-staggered cell average

$$s_j^{t+\Delta t_c} = \frac{1}{2}\,(s_{j+\frac{1}{2}}^{t+\Delta t_c} + s_{j-\frac{1}{2}}^{t+\Delta t_c}) + \frac{1}{8}\,(s'^{\,t+\Delta t_c}_{\,j-\frac{1}{2}} - s'^{\,t+\Delta t_c}_{\,j+\frac{1}{2}}). \tag{21}$$

(Here $s_j^{t+\Delta t_c} \equiv s_j(t + \Delta t_c)$.)

Remarks:

1) The NT central differencing scheme for the approximation of the hyperbolic conservation law (8) can be written in the form of three separate steps: a prediction step (18), a correction step (17), and projection step (21).

2) The numerical derivatives that appear in equations (17), (18), and (21) should obey the accuracy constraints (12) and (19). The second-order accurate correction step (17) augments the first-order accurate prediction step (18), and results in a high-resolution second-order central difference approximation of (8).

3) To guarantee the desired non-oscillatory property of these approximations, the numerical derivatives $\frac{1}{\Delta x}s'_j$ and $\frac{1}{\Delta x}f'_j$ must be carefully chosen [24] (see [3] for our choice).

4) To solve the hyperbolic subsystem associated to the system (1)-(4) we use a component-wise extension [24] of the NT scheme for scalar equations discussed above.

5) The CFL condition for the subsystem of hyperbolic conservation laws assumes the form

$$\frac{\Delta t_c}{\Delta x}\max_{x_j\le x\le x_{j+1}}\rho\left(\frac{1}{\phi(x)}J(f_w,f_g)\right) < \frac{1}{2}, \tag{22}$$

where $\rho(A)$ denotes the spectral radius of matrix A and $J(f_w, f_g)$ is the Jacobian matrix of the fractional flow functions associated to the system (1)-(4).

3.2 Numerical approximation of the diffusive system with variable porosity field

We discuss a numerical procedure in two space dimensions that we employ for the solution of the parabolic subsystem associated to the system (1)-(4). This procedure combines a domain decomposition technique with an implicit time backward Euler method (see [3]) in the construction of an efficient iterative method which allows for variable porosity.

We consider an element-by-element domain decomposition and require that the pairs $(S_{w_j}, \mathbf{w}_{w_j})$ and $(S_{g_j}, \mathbf{w}_{g_j})$ (where $S_{i_j} = S_i|_{\Omega_j}$, $i = w,\ g.$) be a solution of the subsystem associated with (1)-(4) for $\mathbf{x} \in \Omega_j$, $j = 1, \ldots, M$. It is also necessary to impose the consistency conditions,

$$\begin{array}{cc} S_{w_j} = S_{w_k}, & S_{g_j} = S_{g_k} \quad \mathbf{x} \in \Gamma_{jk}, \\ \mathbf{w}_{w_{jk}}\cdot\nu_j + \mathbf{w}_{w_{kj}}\cdot\nu_k = 0, & \mathbf{w}_{g_{jk}}\cdot\nu_j + \mathbf{w}_{g_{kj}}\cdot\nu_k = 0,\ \mathbf{x} \in \Gamma_{jk}, \end{array} \tag{23}$$

where ν_j is a outward normal unit vector of the element Ω_j.

In order to define an iterative method to solve the above problem, it will be convenient to replace the consistency conditions in Eq. (23) by the equivalent Robin transmission boundary conditions [12]. These consistency conditions are given by

$$-\chi_{w_{jk}}\mathbf{w}_{w_j}\cdot\nu_{j_j} + S_{w_j} = \chi_{w_{jk}}\mathbf{w}_{w_k}\cdot\nu_{j_k} + S_{w_k}, \quad \mathbf{x} \in \Gamma_{jk} \subset \partial\Omega_j, \tag{24}$$

$$-\chi_{w_{kj}}\mathbf{w}_{w_k}\cdot\nu_{j_k} + S_{w_k} = \chi_{w_{kj}}\mathbf{w}_{w_j}\cdot\nu_{j_j} + S_{w_j}, \quad \mathbf{x} \in \Gamma_{kj} \subset \partial\Omega_k, \tag{25}$$

$$-\chi_{g_{jk}}\mathbf{w}_{g_j}\cdot\nu_{j_j}+S_{g_j}=\chi_{g_{jk}}\mathbf{w}_{g_k}\cdot\nu_{j_k}+S_{g_k},\qquad \mathbf{x}\in\Gamma_{jk}\subset\partial\Omega_j, \tag{26}$$

$$-\chi_{g_{kj}}\mathbf{w}_{g_k}\cdot\nu_{j_k}+S_{g_k}=\chi_{g_{kj}}\mathbf{w}_{g_j}\cdot\nu_{j_j}+S_{g_j},\qquad \mathbf{x}\in\Gamma_{kj}\subset\partial\Omega_k, \tag{27}$$

where $\chi_{w_{jk}}$ and $\chi_{g_{jk}}$ are positive functions on Γ_{jk} (see [12]).

We consider the lowest index Raviart-Thomas space [23] over Ω_j to approximate the pairs $(S_w,\mathbf{w}_w)$ and $(S_g,\mathbf{w}_g)$. The degrees of freedom on an element Ω_j are the values S_{w_j} and S_{g_j} and the two values $w_{w_{j_\beta}}$ and $w_{g_{j_\beta}}$, $\beta=L,R,B,T$, of the diffusive fluxes across the edge of the elements. We shall also introduce the Lagrange multipliers ℓ_{w_β} and ℓ_{g_β}, $\beta=L,R,B,T$, for the water and gas saturations, respectively, on Γ_{jk}; these multipliers are constant on each edge.

So, after some standard calculations the discrete form of the parabolic subsystem can be written as (see [1, 11]):

$$\phi_j\left(\frac{S_{w_j}-\bar{S}_{w_j}}{\Delta t_d}\right)-\frac{1}{h_x}\left(w_{w_{j_R}}+w_{w_{j_L}}\right)+\frac{1}{h_y}\left(w_{w_{j_U}}+w_{w_{j_D}}\right)=0, \tag{28}$$

$$w_{w_{j_\beta}}B^{-1}_{11_\beta}+w_{g_{j_\beta}}B^{-1}_{12_\beta}=\frac{2}{h_x}(S_{w_j}-\ell_{w_{j_\beta}}),\quad \beta=L,R, \tag{29}$$

$$w_{w_{j_\beta}}B^{-1}_{11_\beta}+w_{g_{j_\beta}}B^{-1}_{12_\beta}=\frac{2}{h_y}(S_{w_j}-\ell_{w_{j_\beta}}),\quad \beta=B,T, \tag{30}$$

$$\phi_j\left(\frac{S_{g_j}-\bar{S}_{g_j}}{\Delta t_d}\right)-\frac{1}{h_x}\left(w_{g_{j_R}}+w_{g_{j_L}}\right)+\frac{1}{h_y}\left(w_{g_{j_U}}+w_{g_{j_D}}\right)=0, \tag{31}$$

$$w_{w_{j_\beta}}B^{-1}_{21_\beta}+w_{g_{j_\beta}}B^{-1}_{22_\beta}=\frac{2}{h_x}(S_{g_j}-\ell_{g_{j_\beta}}),\quad \beta=L,R, \tag{32}$$

$$w_{w_{j_\beta}}B^{-1}_{21_\beta}+w_{g_{j_\beta}}B^{-1}_{22_\beta}=\frac{2}{h_y}(S_{g_j}-\ell_{g_{j_\beta}}),\quad \beta=B,T, \tag{33}$$

where $B^{-1}_{ij_\beta}$ are the entries of the inverse matrix $B^{-1}(\ell_{w_\beta},\ell_{g_\beta})=(QP')^{-1}(\ell_{w_\beta},\ell_{g_\beta})$. Here a trapezoidal rule is used for the evaluation of the pertinent integrals in the derivation of Eqs. (28)-(30) and Eqs. (31)-(33). To simplicity of notation, in this section ϕ_j means the value of the porosity in the element Ω_j.

Define an iterative scheme for the solution of the parabolic subsystem by applying Eqs. (24)-(25) to Eqs. (29)-(30) and Eqs. (26)-(27) to Eqs. (32)-(33) to express all Lagrange multipliers in terms of Lagrange multipliers and fluxes associated with adjacent elements. This scheme, developed in [1, 3] for constant porosity (see also [11]) is a natural extension for parabolic systems of the procedure introduced in [12] for scalar elliptic and parabolic problems.

The time discretization for the equations (28)-(33) is performed by means of the implicit backward Euler method (see [3]). Note that $\bar{S}_w$ and $\bar{S}_g$ are the initial conditions for the diffusive (discrete form) system (28)-(33).

4 Numerical Experiments

We consider the following Riemann problem for the numerical experiments reported in this work:

$$S_w^L=0.721\qquad S_g^L=0.279\quad\text{and}\quad S_w^R=0.05\qquad S_g^R=0.15. \tag{34}$$

We take the Leverett model [20] for capillary pressure which is given by

$$p_{wo} = 5\epsilon(2 - S_w)(1 - S_w) \quad \text{and} \quad p_{go} = \epsilon(2 - S_g)(1 - S_g), \tag{35}$$

where the coefficient ϵ controls the relative importance of convective and diffusive forces. We take $\epsilon = 0.001$ and fluid viscosities $\mu_o = 1.0$, $\mu_w = 0.5$, and $\mu_g = 0.3$.

We adopt two distinct sets of relative permeability functions in our numerical experiments. These sets are particular choices of the following expressions

$$k_w = S_w^2, \quad k_o = S_o^2, \quad \text{and} \quad k_g = (1 - \alpha_g)S_g^2 + \alpha_g S_g, \quad 0 \leq \alpha_g \leq 1. \tag{36}$$

By setting the parameter $\alpha_g = 0$ we obtain the classical immiscible Corey-type model for phase relative permeabilities. For this model, the subsystem of conservation laws modeling phase convection loses strict hyperbolicity at a particular point in the interior of the saturation triangle, whose location is determined by the fluid viscosities. It is well known that non-classical transitional shock waves typically arise in solutions of this model, and that their correct computation requires the precise modeling of capillarity effects. See [6] for some experimental evidence of the occurrence of transitional shock waves.

Following [16], any choice

$$\alpha_g > \frac{\mu_g}{\sqrt{\mu_w \, \mu_o}} \tag{37}$$

leads to a strictly hyperbolic subsystem of conservation laws for the convective transport of fluid phases.

The boundary conditions and injection and production specifications for three-phase flow equations (1)-(7) are as follows. For the horizontal slab geometry (Figure 2), injection is performed uniformly along the left edge ($x = 0$ m) of the reservoir (see top picture in Figure 2) and the (total) production rate is taken to be uniform along the right edge ($x = 512$ m); no flow is allowed along the edges appearing at the top and bottom of the reservoir. In the case of a five-spot geometry (Figure 3), injection takes place at one corner and production at the diametrically opposite corner; no flow is allowed across the entirety of the boundary. In the simulations reported in Figures 2, 3, and 4 (right column) the Corey-type model was used ($\alpha_g = 0$).

Note in Figure 3 that low porosity region drives a fast finger towards this region (see top left picture in Figure 3). This finger is better resolved under refinement (see bottom left and right pictures in Figure 3).

For the study reported in Figure 2 we consider a scalar absolute permeability field $K(\mathbf{x})$ taken to be log-normal (a fractal field, see [14] and references therein for more details) with moderately large heterogeneity strength. The spatially variable permeability field is defined on 512×128 grid with the coefficient of variation C_v (standard deviation)/mean: 0.5. The porosity field is piecewise constant with two distinct alternating values, 0.1 and 0.3 (see top picture in Figure 2).

Next we turn to a 1D comparison between the two models for phase relatives permeabilities. Figure 4 shows that the numerical solution of (1)-(7) with

Riemann problem data (34) for the Corey-type model ($\alpha_g = 0$) a transitional shock wave is simulated (right) which is not present in the solution model with $\alpha_g = 0.43$ (left) that leads to a strictly hyperbolic subsystem of conservation laws modeling the convective transport of fluid phases for three-phase flow.

5 Conclusions

We described the development of a numerical simulation tool for three-phase immiscible incompressible flow. The porous medium may be heterogeneous with variable porosity and permeability fields. General relations for the relative permeability functions may also be used. It may lead to the loss of strict hyperbolicity and, thus, to the existence of an elliptic region or an umbilic point for the system of nonlinear hyperbolic conservation laws describing the convective transport of the fluid phases.

We reiterate that transitional waves are related to the immiscible Corey-type model for phase relative permeabilities and to the existence of an umbilic point and it has a strong dependency upon the physical diffusion being modeled (see [15] and references therein). Thus, their accurate computation constitutes a difficult test for numerical simulators.

This numerical procedure has been used to investigate the existence and stability of non-classical waves (also called transitional or undercompressive waves) in heterogeneous two-dimensional flows, thereby extending previous results for one-dimensional problems.

Acknowledgments. E.A. thanks CAPES/Brazil (IPRJ/UERJ) for a Ph.D. Fellowship. F.F. was supported by NSF grant INT-0104529. F.P. was supported by CNPq grants 472199/01-3, CTPetro/CNPq, 470216/2003-4, 504733/2004-4, and CNPq/NFS grant 490696/2004-0.

References

1. Abreu, E.: Numerical simulation of three-phase water-oil-gas flows in petroleum reservoirs. Universidade do Estado do Rio de Janeiro, M.Sc Thesis (2003) (in Portuguese - Available at http://www.labtran.iprj.uerj.br/Orientacoes.html)
2. Abreu, E., Furtado, F., Pereira, F.: On the Numerical Simulation of Three-Phase Reservoir Transport Problems. Transport Theory and Statistical Physics, **33** (5-7) (2004) 503–526
3. Abreu, E., Douglas, J., Furtado, F., Marchesin, D., Pereira, F.: Numerical Simulation of Transitional Waves in Three-Phase Oil-water-gas Immiscible Displacement in Porous Medium (To appear in Journal of Applied Numerical Mathematics)
4. Abreu, E., Furtado, F., Marchesin, D., Pereira, F.: Transitional Waves in Three-Phase Flows in Heterogeneous Formations. *Computational Methods for Water Resources*, Edited by C. T. Miller, M. W. Farthing, W. G. Gray and G. F. Pinder, Series: Developments in Water Science, **I**, (2004) 609–620
5. Berre, I., Dahle, H. K., Karlson, K. H., Nordhaug, H. F.: A streamline front tracking method for two- and three-phase flow including capillary forces. *Contemporary Mathematics: Fluid flow and transport in porous media: mathematical and numerical treatment*, **295** (2002) 49–61

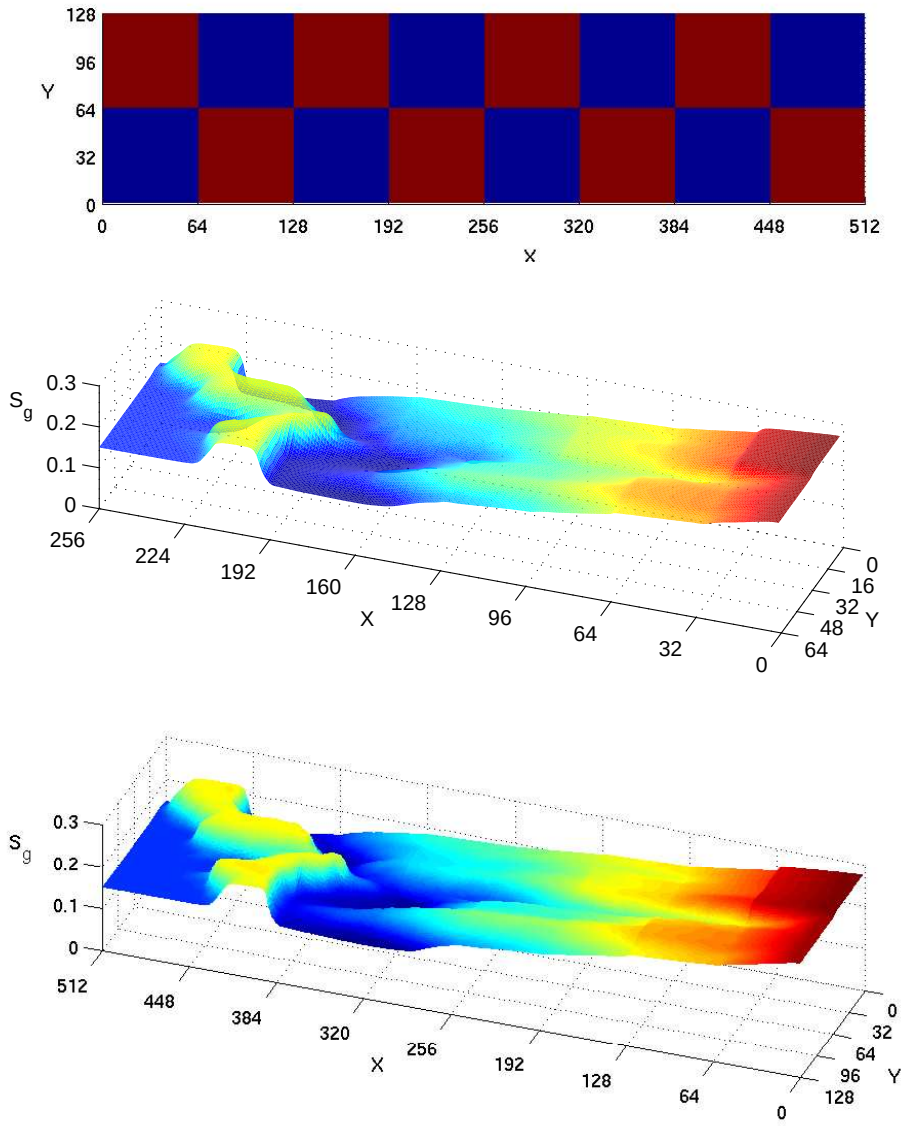

Fig. 2. Mesh refinement study for the gas saturation surface for three-phase flow after 920 days of simulation. The reservoir has 512 m $\times$ 128 m and $C_v = 0.5$. The porosity field is piecewise constant with two distinct alternating values 0.1 (blue) and 0.3 (red) (top picture). Computational grids: 256 $\times$ 64 (middle) and 512 $\times$ 128 (bottom).

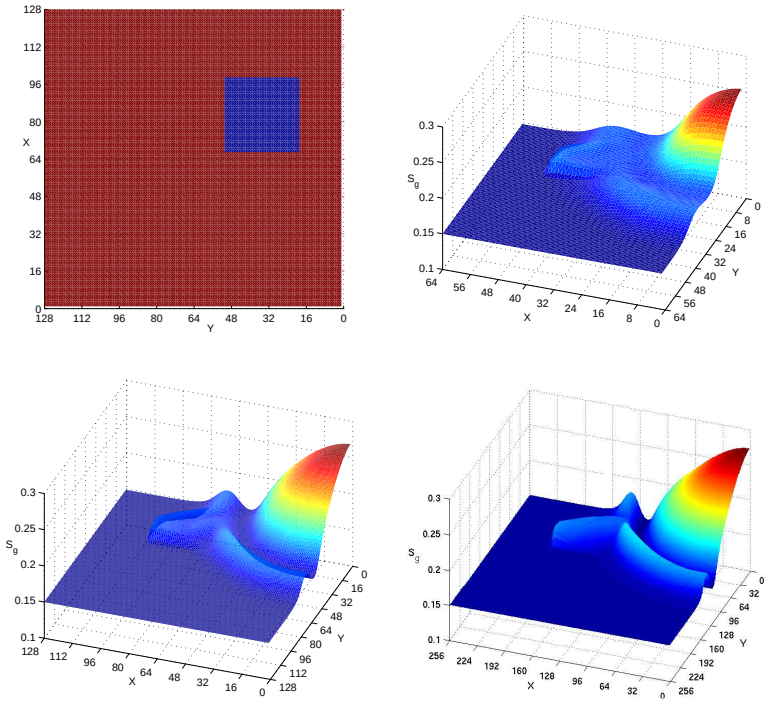

Fig. 3. Mesh refinement study in a 5-spot pattern reservoir after 250 days of simulation. The porosity field (top left) is piecewise constant with only two distinct values: 0.002 in a small rectangular region where the finger develops and 0.2 elsewhere. The 128 m $\times$ 128 m reservoir is discretized with computational grid having 64 $\times$ 64 (top right), 128 $\times$ 128 (bottom left), and 256 $\times$ 256 (right left) elements.

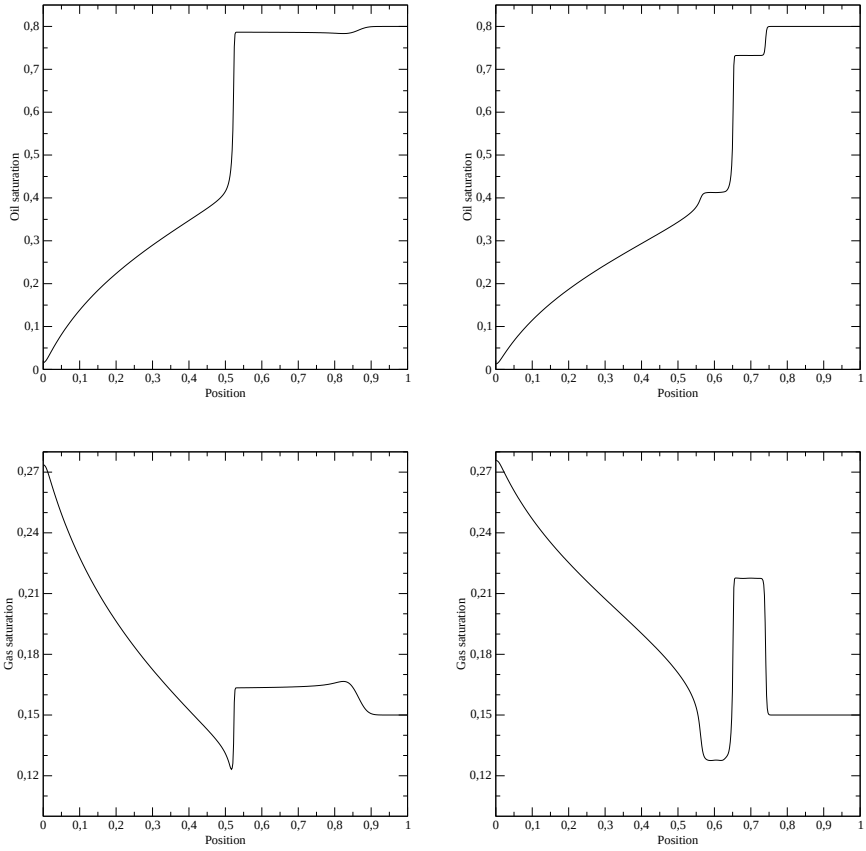

Fig. 4. Oil and gas saturation profiles are shown as a function of dimensionless distance from top to bottom at time 750 days for two models of phase relative permeabilities. We remark that for the choice $\alpha_g = 0$ a transitional (intermediate) shock wave is simulated (right) which is not present in the solution model of phase relative permeabilities with $\alpha_g = 0.43$ (left) that leads to a strictly hyperbolic subsystem of conservation laws.

6. Bruining, J., Duijn, C.J. van.: Uniqueness Conditions in a Hyperbolic Model for Oil Recovery by Steamdrive. Computational Geosciences (February 2000), **4**, 65–98
7. Chen, Z., Ewing, R. E.: Fully-discrete finite element analysis of multiphase flow in ground-water hydrology. *SIAM J. on Numerical Analysis.* **34**, (1997) 2228–2253
8. Chorin, A. J., Hughes, T. J. R., McCraken, M. F., and Marsden, J. E.: Product Formulas and Numerical Algorithms. *Comm. Pure Appl. Math.*. **31**, (1978) 205–256
9. Colella, P., Concus, P., and Sethian, J.: Some numerical methods for discontinuous flows in porous media. The Mathematics of Reservoir Simulation. *SIAM Frontiers in Applied Mathematics 1.* Edited by Richard E. Ewing, (1984) 161–186
10. Corey, A., Rathjens, C., Henderson, J., Wyllie, M.: Three-phase relative permeability. *Trans. AIME*, **207**, (1956) 349–351
11. Douglas, Jr. J., Furtado, F., Pereira, F.: On the numerical simulation of waterflooding of heterogeneous petroleum reservoirs. *Comput. Geosci.*, **1**, (1997) 155–190
12. Douglas, Jr. J., Paes Leme, P. J., Roberts, J. E. and Wang, J.: A parallel iterative procedure applicable to the approximate solution of second order partial differential equations by mixed finite element methods. *Numer. Math.*, **65**, (1993) 95–108
13. Dria, D. E., Pope, G.A, Sepehrnoori, K.: Three-phase gas/oil/brine relative permeabilities measured under CO_2 flooding conditions. *SPE 20184*, (1993) 143–150
14. J. Glimm, B. Lindquist, F. Pereira, and R. Peierls.: The fractal hypothesis and anomalous diffusion. *Computational and Applied Mathematics*, **11** (1992) 189–207
15. Isaacson, E., Marchesin, D., and Plohr, B.: Transitional waves for conservation laws. *SIAM J. Math. Anal.*, **21**, (1990), 837–866
16. Juanes, R., Patzek, T. W.: Relative permeabilities for strictly hyperbolic models of three-phase flow in porous media. *Transp. Porous Media*, **57** No. 2 (2004) 125-152
17. Juanes, R., Patzek, T. W.: Three-Phase Displacement Theory: An Improved Description of Relative Permeabilities. *SPE Journal.* **9**, No. 3, (2004) 302–313
18. Karlsen, K. H, Risebro, N. H.: Corrected operator splitting for nonlinear parabolic equations. SIAM Journal on Numerical Analysis, **37** No. 3, (2000) 980-1003
19. Karlsen, K. H, Lie, K.-A., Natvig, J. R., Nordhaug, H. F., and Dahle, H. K.: Operator splitting methods for systems of convection-diffusion equations: nonlinear error mechanisms and correction strategies. *J. of Computational Physics*, **173**, Issue 2, (2001) 636-663
20. Leverett, M. C., Lewis, W. B.: Steady flow of gas-oil-water mixtures through unconsolidated sands. *Trans. SPE of AIME*, **142**, (1941) 107–16
21. Li, B., Chen, Z., Huan, G.: The sequential method for the black-oil reservoir simulation on unstructured grids. *J. of Computational Physics*, **192**, (2003) 36–72
22. Marchesin, D., Plohr, B. J.: Wave structure in WAG recovery. SPE 71314, *Society of Petroleum Engineering Journal*, **6**, no. 2, (2001) 209–219
23. Raviart P-A., Thomas, J. M.: A mixed finite element method for second order elliptic problems. *Mathematical Aspects of the Finite Element Method*, Lecture Notes in Mathematics, Springer-Verlag, Berlin, New York, I. Galligani, and E. Magenes, eds. **606** (1977) 292–315
24. Nessyahu, N., Tadmor, E.: Non-oscillatory central differencing for hyperbolic conservation laws. *J. of Computational Physics*, (1990) 408–463
25. Peaceman, D. W.: Fundamentals of Numerical Reservoir Simulation. Elsevier, Amsterdam (1977)
26. Stone, H. L.: Probability model for estimating three-phase relative permeability. *Petrol. Trans. AIME, 249. JPT*, **23**(2), (1970) 214–218